Shape Optimization of Damping Layers

T.-C. Lin
R. A. Scott

Shape optimization of unconstrained and constrained damping layers is treated. The specific problem analyzed is a cantilever beam loaded at its tip by a harmonic force. Finite element modeling and mathematical programming techniques are used to obtain the solution. Performance measures are taken to be reduction of maximum displacement and increase in fatigue lifetime. Results include the improvement, over the uniform treatment case, of these measures when the profile of the damping layer is optimized.

INTRODUCTION

Treatment of vibration problems by damping layers, both constrained and unconstrained is quite common. Early work in the field can be found in Ross, Ungar and Kerwin [1]. More recently, finite element techniques have been used to address the problem. Papers relevant to the present work are those of Johnson, Kienholz and Rogers [2], Johnson and Kienholz [3], Soni and Bogner [4], and Soni [5].

Advances have also been made recently on the structural optimization front. Improvements in design sensitivity analysis were given by Kim, Anderson and Sandstrom [6]. Shape optimization techniques using pure finite element modeling were presented by Kikuchi, Chung, Torigaki and Taylor [7]. Of note is the work of Niordson [8], who showed the importance of imposing a slope constraint in the optimum design of elastic plates. Viscoelastic materials have also been treated. A study quite closely related to the theme of the present paper was given by Lekszycki and Olhoff [9], who analyzed shape optimization of an elastic beam covered by an unconstrained viscoelastic layer. Using calculus of variation techniques, they obtained an explicit optimality condition, which was solved in an iterative fashion.

Here shape optimization is considered for both constrained and unconstrained layers on a beam. A key question addressed is, for a given volume of material, how much improvement can be obtained, over the uniform treatment case, if the profile of the damping layer is allowed to vary and be optimized. The specified problem treated involves a cantilever beam loaded at its tip by a time harmonic force. Performance measures are taken to be reduction in maximum displacement, and improvement in fatigue lifetime. Finite element modeling, together with numerical approaches to the complex eigenvalue problem and mathematical programming techniques are used to obtain the solution.

It should be noted that complete details are not presented in the paper (these can be found in [10]). The work focuses on the essential ideas and on the results.

MECHANICAL MODELING

Only a single constrained layer is treated here and the basic configuration is sketched in Fig. 1. The mechanical modeling used is traditional. The basic

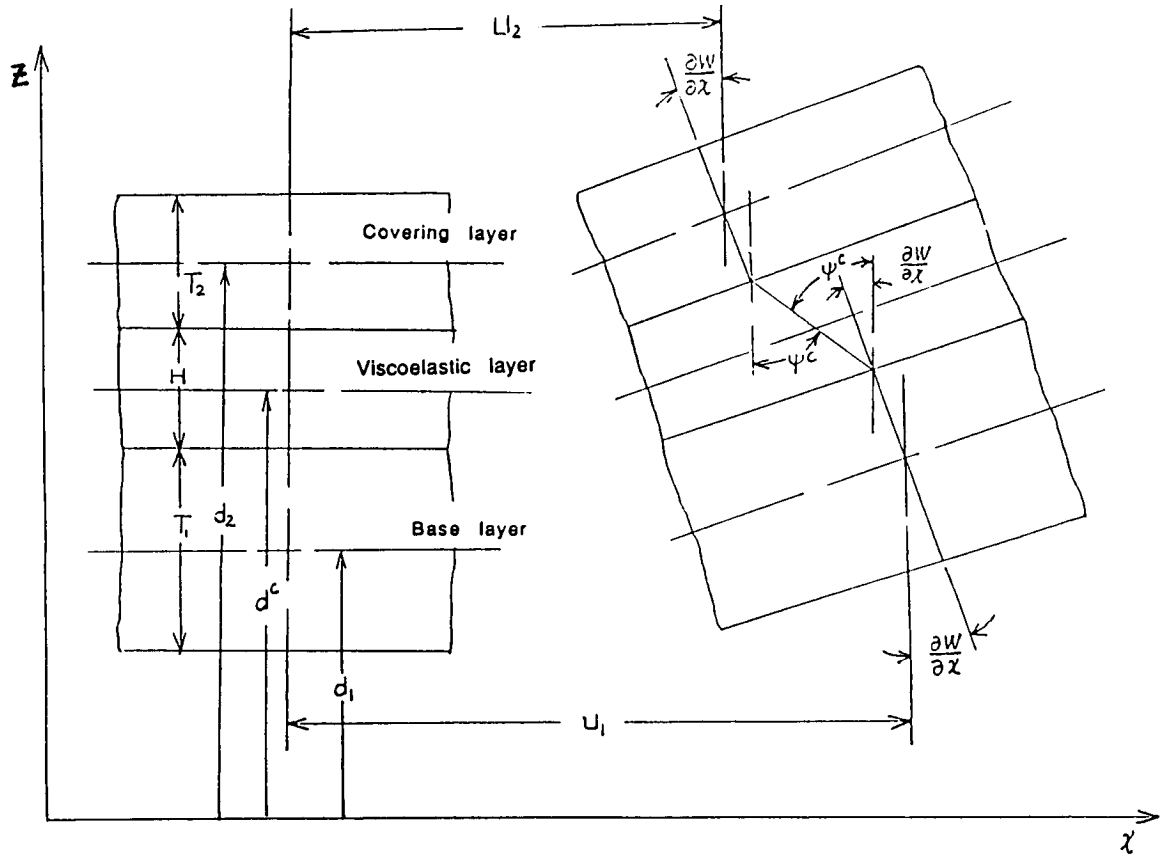

Figure 1. Basic Configuration of a Three-Layered Beam

beam and constraining layer are taken to be Euler-Bernoulli beams and the damping layer, for which shear is important, is treated as a Timoshenko beam. Perfect bonding is assumed. With this modeling, the displacement components are given by

$$\bar{U}(x,z,t) =$$

$$U_1(x,t)-(z-d_1)W_{,x}(x,t),\ d_1-T_1/2\le z\le d_1+T_1/2,\ \text{base layer} \tag{1}$$

$$U_2(x,t)-(z-d_2)W_{,x}(x,t),\ d_2-T_2/2\le z\le d_2+T_2/2,\ \text{covering layer} \tag{2}$$

$$U^c(x,t)-(z-d^c)\psi^c(x,t),\ d^c-H/2\le z\le d^c+H/2,\ \text{damping layer} \tag{3}$$

$$\bar{W}(x,z,t) = W(x,t) \tag{4}$$

$$U^c(x,t) = (1/2)(U_1(x,t)+U_2(x,t))+(1/4)(T_2-T_1)W_{,x} \tag{5}$$

$$\psi^c(x,t) = (1/H)(U_1(x,t)-U_2(x,t))-(1/2H)(T_1+T_2)W_{,x} \tag{6}$$

In the above, U_1, U_2, and U^c are the midplane longitudinal displacements of the base beam, covering layer and core, respectively.

The relevant, non-zero strains are

$$\varepsilon_{x1} = U_{1,x} - (z-d_1)W_{,xx} \tag{7}$$

$$\varepsilon_{x2} = U_{2,x} - (z-d_2)W_{,xx} \tag{8}$$

$$\varepsilon_x^c = (U_{1,x}+U_{2,x})/2+(T_1-T_2)W_{,xx}/4 + (z-d_c)[U_{2,x}-U_{1,x})/H + (T_1+T_2)W_{,xx}/2H] \tag{9}$$

$$\gamma_{xz}^c = -\psi^c + W_{,x} \quad , d^c-H/2 \leq z \leq d^c+H/2 \tag{10}$$

For the base beam and covering layer, the stress strain relations are

$$\sigma_{x1} = E_1\varepsilon_{x1} \tag{11}$$

$$\sigma_{x2} = E_2\varepsilon_{x2} \tag{12}$$

where E denotes Young's modulus. The damping layer is treated as a Kelvin solid, for which the stress-strain relations are

$$\sigma_x^c = E^c\varepsilon_x{}^c + \zeta_1^c\,\dot{\varepsilon}_x^c \tag{13}$$

$$\sigma_{xz}{}^c = G^c\gamma_{xz}^c + \eta_1{}^c\,\dot{\gamma}_{xz}^c \tag{14}$$

where G^c stands for the shear modulus of the core and $\zeta_1{}^c$, $\eta_1{}^c$ are material parameters characterizing the viscoelasticity. For harmonic loading, such as is being considered here, the complex modulus approach is adopted. Then

$$\sigma_x{}^c = E^*\varepsilon_x{}^c \tag{15}$$

$$\sigma_{xz}{}^c = G^*\gamma_{xz}^c \tag{16}$$

where

$$G^* = \text{complex shear modulus of the damping layer} = G^c(1+i\eta^c) \tag{17}$$

$$E^* = \text{complex Young's modulus of the damping layer}$$
$$= E^c(1+i\zeta^c) \tag{18}$$

where η^c and ζ^c are the loss factors for the damping material. For harmonic motion of frequency ω, the relationships between the Kelvin parameters and the loss factors are

$$G^c = E^c/(2(1+\nu^c)) \tag{19}$$

$$\eta^c = \eta_1^c\ \omega/G^c \tag{20}$$

$$\zeta^c = \zeta_1^c\ \omega/E^c \tag{21}$$

In the sequel, following Nashif, Jones and Henderson [11], Poisson's ratio ν^c is taken to be a constant.

Equations (1) through (21) essentially set forth the mechanical modeling. The procedure then is straightforward. The principle of virtual work states:

$$\int_v(\sigma_x\delta\varepsilon_x + \sigma_{xz}\delta\gamma_{xz})dv + \delta V_I - \delta V_s = 0 \tag{22}$$

where δV_I and δV_s denote virtual work by the inertia forces and surface tractions, respectively. Using eqs. (1) through (21) in eq. (22) leads to an integral expression involving the "degrees of freedom" U_1, U_2, W, $\partial W/\partial x$. This expression is then discretized using a finite element method. Note that similar modeling can be done for an arbitrary number of layers.

FINITE ELEMENT MODELING

Using eqs. (1) through (6), it can be shown that the volume integrals in eq. (22) reduce to line integrals in the x-direction. These integrals are then discretized using finite elements of length L_e. Rod elements are used for axial displacements. Specifically, the shape functions are given by:

$$U_i(x) = [(1-x/L_e)\ x/L_e][(U_i^1\ U_i^2)]^T \tag{23}$$

where i = 1, 2 indicate base beam and covering layer, respectively, and U_i^1, U_i^2 are nodal displacements. Beam elements are used to handle the transverse deformations, with shape functions given by

$$W(x) = [N_1\ N_2\ N_3\ N_4][W^1\ \ \theta^1\ W^2\ \ \theta^2\ ]^T \tag{24}$$

where $\theta \equiv \frac{\partial W}{\partial x}$, and

$$N_1 = 1 - 3x^2/L_e^2 + 2x^3/L_e^3$$

$$N_2 = x - 2x^2/L_e + x^3/L_e^2$$

$$N_3 = 3x^2/L_e^2 - 2x^3/L_e^3$$

$$N_4 = -(x^2/L_e - x^3/L_e^2) \tag{25}$$

Again in eq. (24), superscripts indicate nodal quantities.

Standard finite element methodology now applies. For harmonic forcing the procedure ultimately leads to, on assembling the various element matrices,

$$-\omega^2[M]\,\underline{X} + i[C]\,\underline{X} + [K]\,\underline{X} = \underline{F} \tag{26}$$

where $\underline{X}$ is a vector of nodal parameters and $\underline{F}$ is a vector of nodal forces (magnitudes). The stiffness, mass and damping matrices, [K], [M], and [C] are lengthy, but straightforward expressions and will not be reproduced here. Note that the form i[C] for the damping matrix, which is frequency dependent, arises from use of the complex modulus approach.

FATIGUE LIFE TIME CALCULATIONS

Here the approach set forth in the SAE document, Ref. [12] is followed. In reality localized plastic flow occurs in fatigue and the nominal stresses and strains, σ and ε, should be replaced by the actual quantities S and e. Neuber introduced the following empirical rule

$$e = \frac{\sigma_{max}^2}{SE} \tag{27}$$

This equation has two unknowns, e and S, and the other needed relationship is the cyclic stress-strain curve for the material, which is curve-fitted by

$$e = \frac{S}{E} + \left(\frac{S}{K'}\right)^{\frac{1}{n'}} \tag{28}$$

where K' and n' are material parameters. Eqs. (27) and (28) are then solved iteratively to obtain S_{max}. The number of cycles to failure N_f is calculated from another empirical relationship, namely:

$$S_{max} = \sigma_f'(2N_f)^b \tag{29}$$

where σ_f' and b are material parameters. Later in the paper an aluminum alloy (AL3015) is studied and for this material the parameters are

$E = 1.0 \times 10^4$ ksi

$K' = 28.6$ ksi

$n' = 0.093$

$\sigma_f' = 38.4$ ksi

$b = -0.088$

OPTIMIZATION PROBLEM

The optimization task is to find a vector b of design variables H_i, $i = 1,2...$ ...n, where H_i is the thickness of the damping layer in the i^{th} finite element, which will minimize the objective function f, here taken to be:

$$f: \quad \min\ (\max|R_j|) \qquad j = 1,2,.....N,$$

where R_j represents the deflection response at node j, subject to the constraints:

volume constraint of damping layer $\quad V_0 - V = 0$

and inequality constraints:

$$H_i \geq 0$$

$H_i^u - H_i \geq 0$, where H_i^u is an upper bound for H_i:

slope constraints:

$$H_v - \left|\frac{\partial H_i}{\partial x}\right| \geq 0, \ H_v \text{ a specified constant.} \tag{30}$$

The constraint on the gradient in eq. (30) needs some explanation. The idea was introduced by Niordson [8] in a study on optimization of elastic plates. He pointed out that without it, exotic shapes (tending towards ribbed structures, with extremely thin stiffeners) would be generated. Apart from the practicality of such structures, the underlying theory (Kirchoff plate theory) is not valid for such rapidly varying shapes. To preserve the underlying theory, he restricted the design space to plates of slowing varying thickness, by means of a slope constraint.

In the current work, the numerical approach requires that the constraints be differentiable. Hence the slope constraints are replaced by the equivalent statements:

$$H_v + \frac{\partial H_i}{\partial x} \geq 0 \tag{31}$$

$$H_v - \frac{\partial H_i}{\partial x} \geq 0 \tag{32}$$

One remark should be made. For some unconstrained layers, it was found that the slope constraints were not necessary to obtain smooth shapes. However, the constraints were found to be essential for constrained layers.

Mathematical programming techniques are used here to obtain the solution. A proven, reliable technique is employed. Belegundu and Arora [13] showed that the program SUMT has these features. Moreover, a listing is available in Kuester [14].

To use the program, sensitivity derivatives $\underline{U}_i(\underline{b}_o)$ are required, where

$$\underline{U}_i(b_o) = \left.\frac{\partial \underline{X}}{\partial b_i}\right|_{\underline{b} = \underline{b}_o}, \quad i = 1,2,..... \tag{33}$$

Partial differentiation of eq. (26) can be shown to give

$$\{-\omega^2 [M] + i [C] + [K]\}\underline{U}_i = \underline{R}_p \tag{34}$$

where

$$\underline{R}_p \equiv \omega^2 \frac{\partial [M]}{\partial b_i} \underline{X} - i \frac{\partial [C]}{\partial b_i} \underline{X} - \frac{\partial [K]}{\partial b_i} \underline{X} \tag{35}$$

Note that in the present problems, [M], [K], and [C] have known analytical forms and the derivatives in eq. (35) can be carried out explicitly. Then eq. (34) has the same structure as eq. (26) and can be solved in the same fashion once the latter has been solved.

The constraint equations in problem are simple algebraic expressions and their sensitivity derivatives can also be readily obtained.

NUMERICAL STRATEGY

Eigenvalue extraction was done by means of a subspace iteration technique together with Jacobi's method for matrix diagonalization. Response was calculated using a Gaussian direct elimination method, modified for complex equations. Design sensitivity coefficients were calculated as discussed in connection with eq. (35). Their magnitudes are then fed into the optimization scheme SUMT.

PROGRAM VALIDATION AND RESULTS

To check the accuracy of the finite element modeling, several calculations were done to determine the natural frequencies and loss factors and compared with results of Soni [5]. The comparisons involved a cantilever aluminum beam (7 inches long, .5 inches wide and .06 inches deep) with .06 inches thick aluminum face sheets. The material constants used were $E = 1.0 \times 10^7$ psi and $\rho = 0.1$ lb/in^3. The core

material was ISD468. For this material, the behavior of G^c and η^c with frequency is known. Poisson's ratio ν^c was taken to have the constant value 0.35. It was assumed (also assumed throughout the paper) that the loss factor is the same in dilation and shear, so that $\zeta^c = \eta^c$. Tables 1 and 2 give comparisons of the first six undamped natural frequencies and the ratio $\eta_2^{(r)}/\eta^c$, $\eta_2^{(r)}$ being the modal loss factor, respectively. Overall, quite good agreement is seen, lending confidence to the numerical procedures.

Table 1. Comparison of Natural Frequencies

Mode Number	M. L. Soni [5] (hz)	Present Result (hz)
1	64.70	64.13
2	298.00	296.80
3	748.20	745.80
4	1409.50	1403.70
5	2305.00	2296.00
6	3447.00	3400.00

Table 2. Comparison of the Ratio $\eta_2^{(r)}/\eta^c$

Mode Number	M. L. Soni [5]	Present Result
1	0.2725	0.2840
2	0.2401	0.2450
3	0.1531	0.1560
4	0.0878	0.0896
5	0.0560	0.0572

The optimization phase of the program was checked on the following test problem given by Rosenbrock (see [14]): minimize the objective function f, where

$$f = -x_1 x_2 x_3, \text{ subject to}$$

constraints:

$$0 \leq x_i \leq 42$$

$$0 \leq (x_1 + 2x_2 + 2x_3) \leq 72$$

Rosenbrock gave the solution: $f = -3456.0$, $x_1 = 24$, $x_2 = 12$, $x_3 = 12$. The present method gave $f = -3453.8$, $x_1 = 23.4$, $x_2 = 12.2$, $x_3 = 12$. Very good agreement is seen. This, and the fact that the trends in Lekszycki and Olhoff's [9] work were

reproduced accurately (as will be seen shortly) led to the conclusion that the program was accurate.

Results for unconstrained layers will now be given.

The first material studied is the one used in [9], for which the parameters are: $E^c = 0.1 \times 10^8$ lb/in^2, $\eta^c = 0.5$, $\rho^c = 0.035$ lb/in^3 and for the base layer $E_1 = E^c$, $\rho = 0.1$ lb/in^3. The dimensions are: $T_1 = 0.06$ inches, B (width) = 0.5 inches, L = 7 inches (Soni's example).

Note that this damping material has quite large moduli (perhaps unrealistically so). Moreover, note that, as in Ref. [9], the effects of shear are neglected.

A harmonic force is applied at the tip. The thickness constraint H_i^u is taken to be 0.32 inches. The initial amount of damping material must be specified. A percentage measure is used, namely:

$$\% \text{ volume of damping material} = \frac{\text{volume of damping material}}{\text{volume of base layer}}$$

Figure 2 shows a result for 100% damping using the present methodology, but ignoring shear effects. A symmetric configuration is used with equal amounts of damping material on the top and bottom of the beam. Only the upper layer is shown in the figure. In fact without a constraining layer, shear effects in the core are quite small and can always be neglected so that in effect an Euler-Bernoulli beam is used. The first bending frequency of the composite beam is $\omega_n = 595$ rad/sec and the excitation frequency is $\omega = 20$ rad/sec, so that we have a case of low

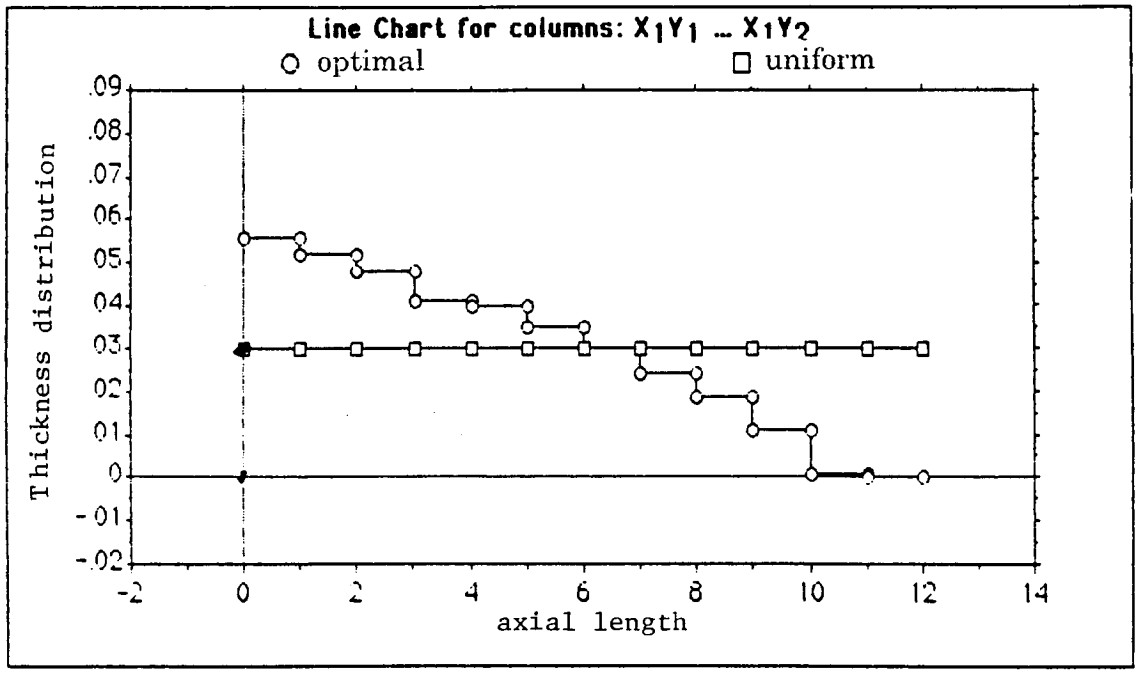

Figure 2. Optimal Shape for High Modulus Material

frequency excitation. The same trend as in Ref. [9] is seen. It is interesting that the present results were obtained without having to specify a constraint on the slope (true for all the results on the unconstrained layers). It was also found that the thickness constraint (0.32 inches) was not active.

Table 3 shows the improvements that can be obtained for various damping treatments. Two kinds of percent reduction in responses are defined by:

$$RRU = \frac{\text{Max. response of bare beam - max. response with uniform damping}}{\text{Max. response of bare beam}}$$

$$RRO = \frac{\text{Max. response of bare beam - max. response with optimal damping}}{\text{Max. response of bare beam}}$$

Table 3. Performance Improvements

% Volume	RRU %	RRO %	Fatigue Life Uniform	Fatigue Life Optimal
100.0	88.6	93.0	0.1775×10^5	0.8764×10^5
66.6	79.9	87.4	0.6722×10^4	0.4270×10^5
33.3	59.4	72.7	0.235×10^4	0.909×10^4
16.6	38.1	58.3	0.129×10^4	0.5994×10^4

Optimization would seem to be worth the trouble. For example, for 33.3% damping an improvement (RRO-RRU) of 13.3% is seen. For 100% damping the improvement is 4.4%. Better fatigue performance is also seen. Optimization led to 39.4% (log value) improvement for 33% damping and 74% improvement for 100% damping.

High frequency excitation was also studied (not treated in Ref. [9]). Figure 3 shows the optimum shape for ω = 750 rad/sec and 100% damping. It is interesting to note that the optimum profile has the opposite trend to that for the low frequency profile.

As a next step in the study, a more realistic material was chosen, namely LORD-400. This is a medium shear modulus material with parameters obtained from Ref. [11]. The natural frequency now is ω_n = 220 rad/sec (based on 100% damping).

The optimal shape for a low frequency excitation (ω = 20 rad/sec) is shown in Figure 4, for a 100% damping material and a bound on thickness of 0.24 inches. Note that the same shape trend is seen, as for the high shear modulus. The thickness changes in Figure 4 are severe and one may question the use of Euler-Bernoulli beam theory. A smaller upper bound on the thickness constraint was used, namely 0.15 inches. The result is shown in Figure 5. A different, smoother shape is seen. This shape dependence on the thickness constraint was not observed for the high modulus material.

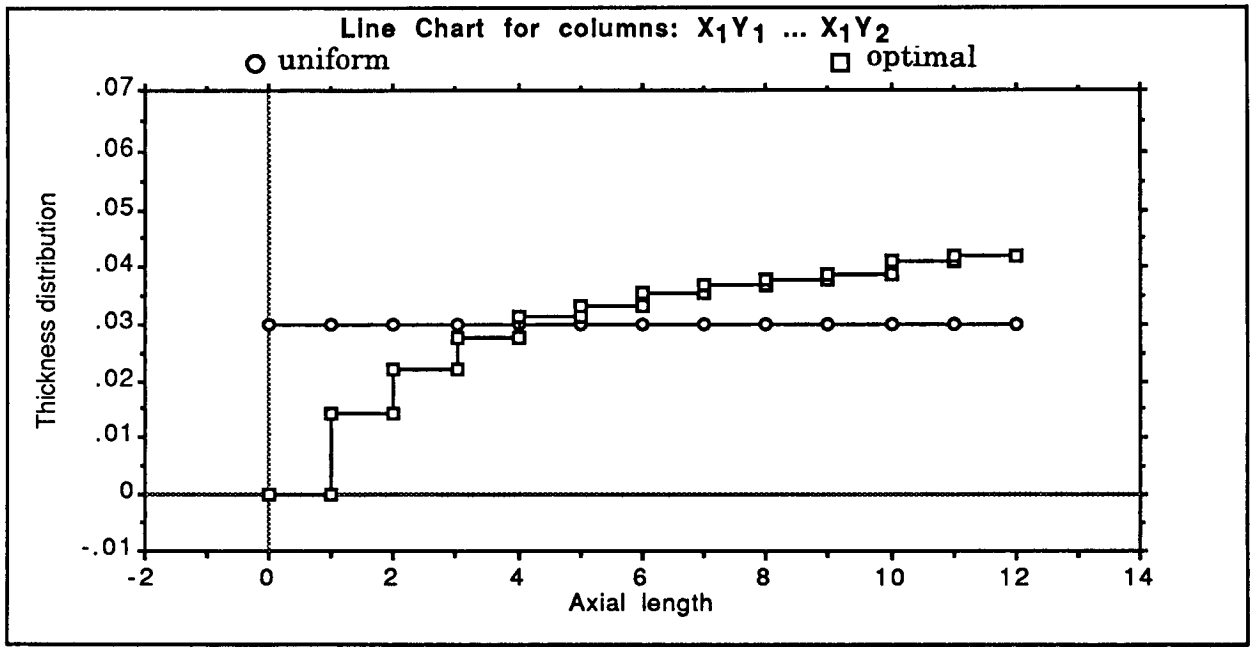

Figure 3. Optimal Shape at High Frequency

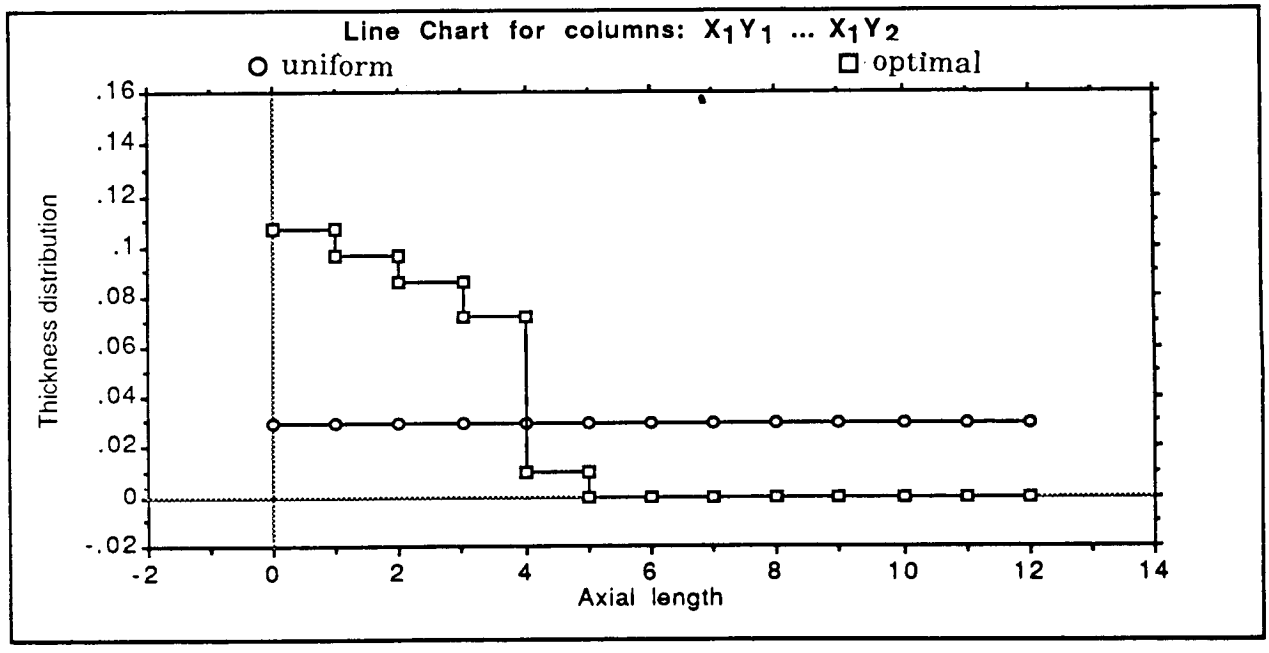

Figure 4. Optimal Shape (LORD-400) for Large Upper Bound

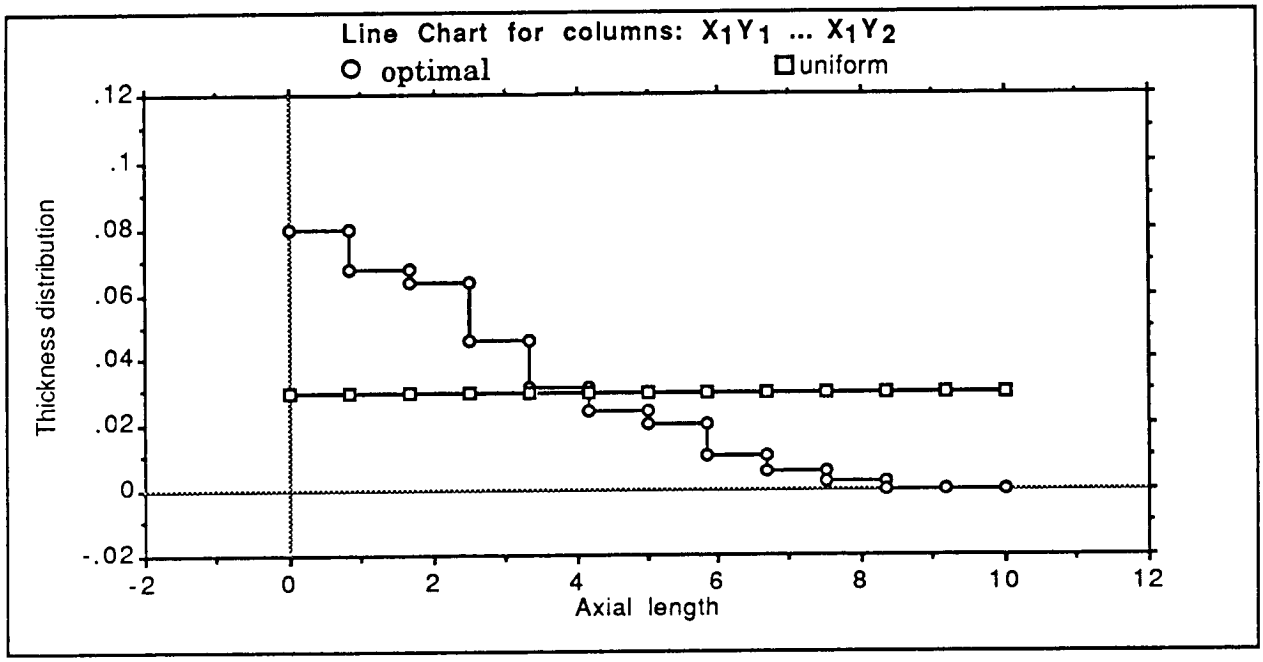

Figure 5. Optimal Shape (LORD-400) for Small Upper Bound

Using the lower upper bound, the following values were found for performance improvement: at 100% damping, RRU = 9.0%, RRO = 19.0%; at 66.6% damping RRU = 4.7%, RRO = 12.1%; at 33.3% damping, RRU = 2.4%, RRO = 7.0%. Results on fatigue are: at 33.3% and 100% damping, the improvements are 5% and 12%, respectively. Though the gains are not as large as for the high modulus material, optimization still seems attractive.

A typical result for high frequency excitation (ω = 240 rad/sec) is shown in Figure 6, for a thickness upper bound of 0.15 inches and 33% damping.

Note that the same shape reversal as was seen for the high modulus material is found. RRO has the value 24.5% so optimization is also worthwhile at high frequencies.

Constrained layers will now be treated (for LORD-400). The first item that should be mentioned is that now a slope constraint is required. Figure 7 shows a shape obtained without such a constraint. Large oscillations in the profile are seen (as was seen by Niordson [8] in his work on elastic plates). Such shapes are not acceptable within the framework of the current mechanical modeling. It was discovered, like Niordson that a slope constraint led to smoother profiles. A slope constraint was imposed at the element level in the form

$$\left| H_{i+1} - H_i \right| < .25\ H_o \qquad i = 1,2,.....N-1$$

where H_o is the thickness of the original uniform damping layer. The thickness of the covering layer is taken to be 10% of the thickness of the damping layer. Only symmetric configurations are considered. A thickness bound of .15 inches was used.

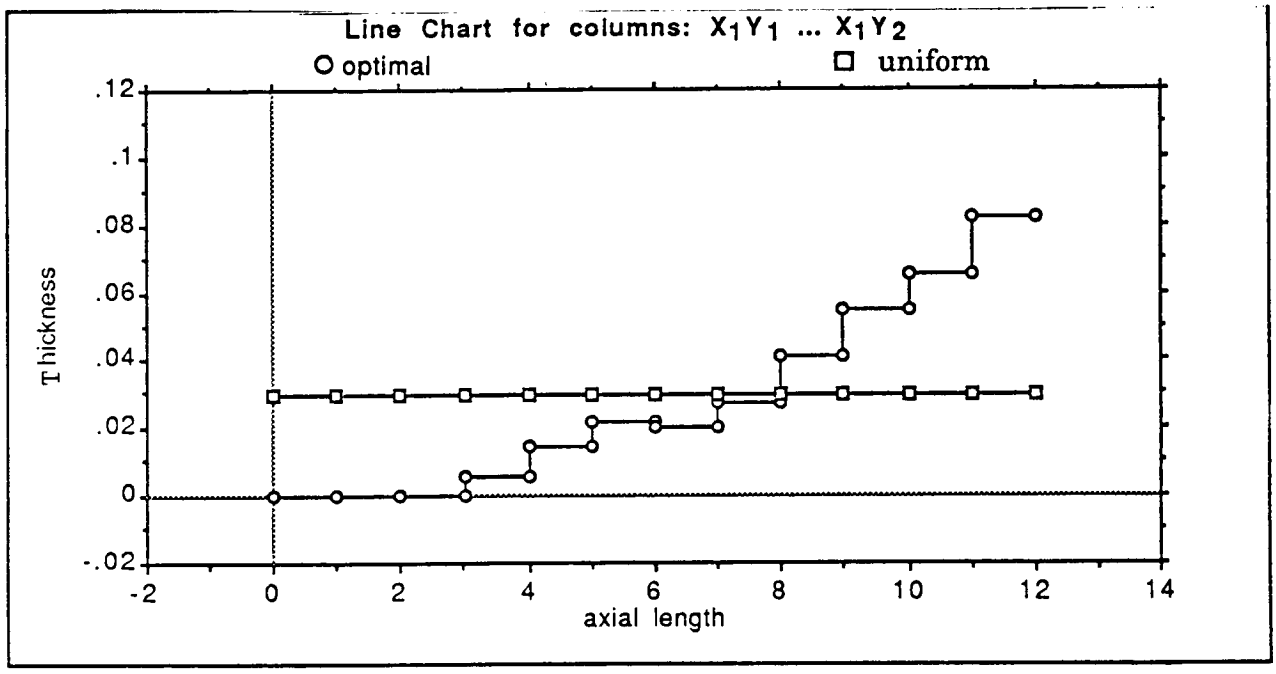

Figure 6. Optimal Shape (LORD-400) for High Frequency Excitation

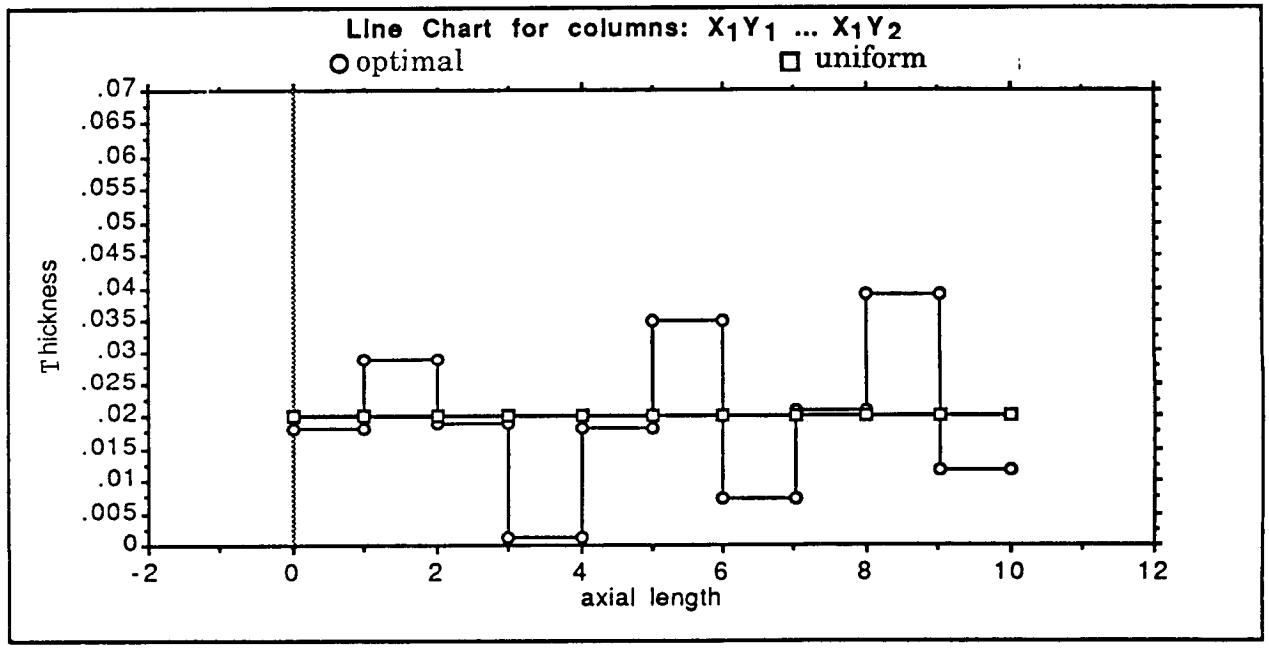

Figure 7. Optimum Shape With No Slope Constraint

An optimum shape for low frequency excitation (ω = 20 rad/sec), is shown in Figure 8 for 100% damping. Comparing this with Figure 5, it is seen that the optimum profiles have opposite trends. One should not anticipate the same trend in both cases. The basic stress at work in the unconstrained damping layer is the bending stress σ_x^c, whereas it is the shear stress σ_{xz}^c in the constrained case.

The improvement in performance (RRO) at 100% damping was found to be 53%. This should be compared with the 19% improvement noted for the unconstrained layer (with the smaller thickness bound). It can be concluded that constrained layers lead to significant improvement in performance.

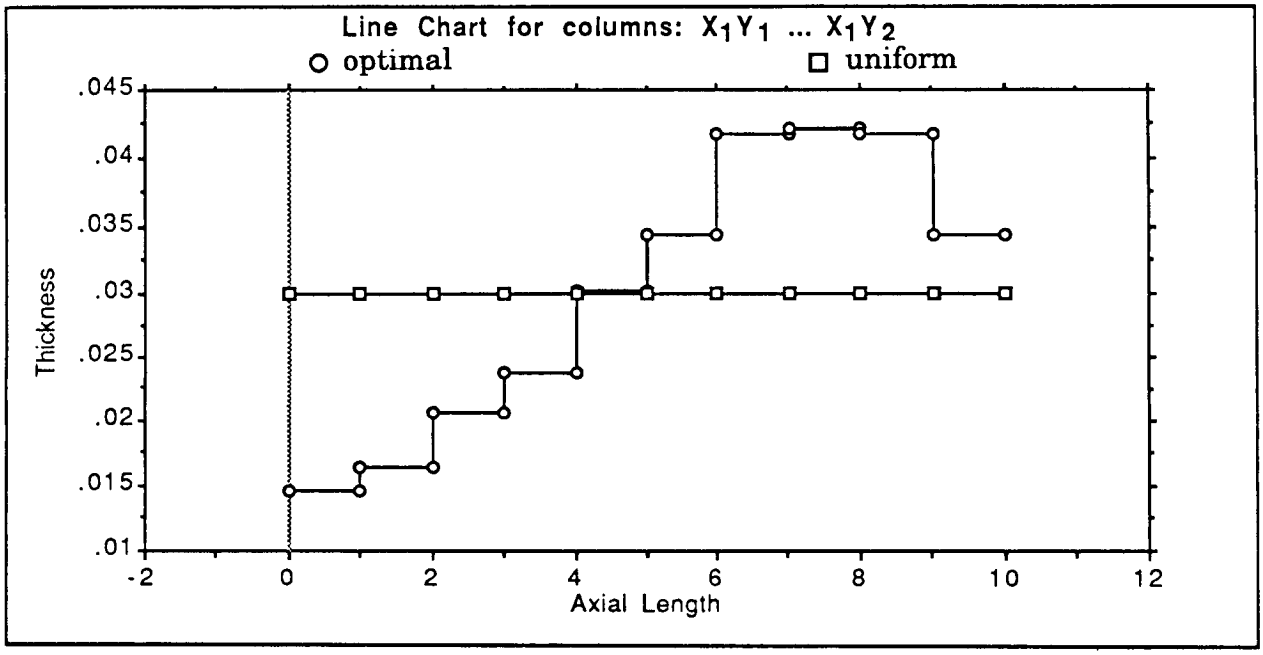

Figure 8. Optimum Shape of a Constrained Damping Layer

REFERENCES

1. D. Ross, E. E. Ungar and E. M. Kerwin, Jr., Damping of Plate Flexural Vibrations by Means of Viscoelastic Laminae, Section 3, ASME Monograph on Structural Damping, 1959.
2. C. D. Johnson, D. A. Kienholz and L. C. Rogers, "Finite Element Prediction of Damping in Beams with Constrained Viscoelastic Layers," Shock Vib. Bull., Vol. 51, Pt. 1, pp. 71-81, May 1981.
3. C. D. Johnson and D. A. Kienholz, "Finite Element Prediction of Damping Layers," AIAA J., Vol. 20, No. 9, pp. 1284-1290, Sept. 1982.
4. M. L. Soni and F. K. Bogner, "Finite Element Vibration Analysis of Damped Structures," AIAA J., Vol. 20, No. 5, pp. 700-707, May 1982.
5. M. L. Soni, "Finite Element Analysis of Viscoelastically Damped Sandwich Structures," Shock. Vib. Bull., Vol. 51, Pt. 1, May 1981.

6. K. O. Kim, W. J. Anderson and R. E. Sandstrom, "Nonlinear Inverse Perturbation Method in Dynamic Analysis, " AIAA J., Vol. 21, No. 9, pp. 1310-1316, Sept. 1983.

7. N. Kikuchi, K. Y. Chung, T. Torigaki and J. E. Taylor, "Adaptive Finite Element Methods for Shape Optimization of Linearly Elastic Structures," Comp. Meth. Appl. Mech. Eng., Vol. 57, pp. 67-89, 1986.

8. F. Niordson, "Optimal Design of Elastic Plates with a Constraint on the Slope of Thickness Function," Int. J. Sol. Struct., Vol. 19, pp. 141-151, 1983.

9. T. Lekszycki and N. Olhoff, "Optimal Design of Viscoelastic Structures Under Forced Steady-State Vibrations," J. Struct. Mech., Vol. 9, pp. 363-387, 1981.

10. T.-C. Lin, Optimal Design of Viscoelastic Structures, Ph.D. Dissertation, Mechanical Engineering, University of Michigan. Submitted, August 1987.

11. A. D. Nashif, D.I.G. Jones and J. P. Henderson, Vibration Damping, John Wiley and Sons, New York, 1985.

12. SAE Standard J1099, pp. 3.59-3.66, 1976.

13. A. D. Belegundu and J. S. Arora, "A Study of Mathematical Programming Methods for Structural Optimization - Part II. Numerical Results," Int. J. Num. Meth. Engng., Vol. 21, pp. 1601-1523, 1985.

14. J. L. Kuester, "Optimization Techniques With Fortran," McGraw-Hill, 1973.